SPRINT, system parameters recurrent invasive tracking: a fast and least-cost online calibration strategy for adaptive optics

Cédric T. Heritier, Thierry Fusco, Sylvain Oberti, Benoit Neichel, Simone Esposito, Pierre-Yves Madec

Monthly Notices of the ROYAL ASTRONOMICAL SOCIETY
MNRAS **504,** 4274–4290 (2021) doi:10.1093/mnras/stab1177

SPRINT, system parameters recurrent invasive tracking: a fast and least-cost online calibration strategy for adaptive optics

C. T. Heritier,[1]★ T. Fusco,[2,3] S. Oberti,[1] B. Neichel,[2] S. Esposito [4] and P.-Y. Madec[1]

[1]*European Southern Observatory, Karl-Schwarzschild-str-2, 85748 Garching, Germany*
[2]*Aix Marseille University, CNRS, CNES, LAM, Marseille, France*
[3]*ONERA, DOTA, Unité HRA, 29 avenue de la division Leclerc, 92322 Chatillon, France*
[4]*INAF - Osservatorio Astrofisico di Arcetri Largo E. Fermi 5, 50125 Firenze Italy*

Accepted 2021 April 21. Received 2021 April 16; in original form 2021 February 15

ABSTRACT

Future large adaptive telescopes will trigger new constraints for the calibration of adaptive optics (AO) systems equipped with pre-focal deformable mirrors (DMs). The image of the DM actuator grid, as seen by the wavefront sensor (WFS), may evolve during the operations because of the flexures of the opto-mechanical components present in the optical path. This will result in a degraded AO performance that will affect the scientific operation. To overcome this challenge, it will be necessary to regularly monitor and compensate for these DM/WFS mis-registrations, either by physically realigning some optical components or by updating the control matrix of the system. In this paper, we present a new strategy to track mis-registrations using a pseudo-synthetic model of the AO system. The method is based on an invasive approach where signals are acquired on-sky, before or during the scientific operations, and fed to the model to extract the mis-registration parameters. We introduce a method to compute the most sensitive modes to these mis-registrations that allows us to reduce the number of degrees of freedom required by the algorithm and to minimize the effect on the scientific performance. We demonstrate that, by using only a few of these well-selected signals, the method provides very good accuracy for parameter estimation, well under the targeted accuracy, and has a negligible effect on the scientific path. In addition, the method appears to be very robust to varying operating conditions of noise and atmospheric turbulence and it performs equally for both pyramid and Shack–Hartmann WFSs.

Key words: instrumentation: adaptive optics – instrumentation: high angular resolution – telescopes – methods: numerical.

1 INTRODUCTION

A large number of ground-based astronomical observations rely on the performance of adaptive optics (AO) systems, which allow us to compensate in real time for the wavefront aberrations induced by atmospheric turbulence. The principle of an AO system consists of measuring signals related to the phase using a wavefront sensor (WFS). These signals are converted by a real-time computer (RTC) into commands to apply to a deformable mirror (DM), which cancels out the optical aberrations. This loop is usually operated in a feedback-l op r,unning at least ten times faster than the typical evolution rate of the atmospheric turbulence.

Within a few years, a new generation of telescopes with diameters up to 39 m, the Extremely Large Telescopes (ELTs), will be in operation. These giant telescopes will address fundamental cases of astrophysical science, such as the direct imaging and characterization of rocky exoplanets located close to their orbiting star or the study of bulk and evolution of the first galaxies (Cirasuolo et al. 2018). The scientific potential of these new telescopes relies on challenging the features of new AO systems, such as the DM integrated inside the telescope itself, and turning the telescopes into adaptive telescopes (Arsenault et al. 2008; Riccardi et al. 2010; Vernet et al. 2012). The colossal size of these large adaptive telescopes and the complexity of their scientific instruments means that there should be a complete rethink to improve both the overall performance and, more specifically, the sensitivity and robustness of the AO systems in order to maximize the astrophysical return of AO-assisted instruments.

In particular, the European Southern Observatory (ESO) ELT (Gilmozzi & Spyromilio 2007) will provide a challenging environment for AO systems. First of all, the calibration of a large number of degrees of freedom (around 5000 actuators; Vernet et al. 2012) with no external calibration source will be required. Furthermore, the use of a pre-focal DM far from the AO instruments with moving elements in the optical path may lead to regular evolution of the DM/WFS registration during the observations (e.g. rotation, shifts or higher order of pupil distortion of the DM actuator grid with respect to the WFS subapertures). These so-called mis-registrations have to be monitored and compensated for, as they will greatly affect the AO performance or could create loop instabilities that will jeopardize the scientific observations.

An illustration of the effect of mis-registrations on the performance of a scientific instrument is given in Fig. 1, which provides simulated *H*-band point spread functions (PSFs) and closed-loop performance for an 8-m telescope equipped with a DM with 21 × 21 actuators and a pyramid WFS w(PWFS) ith 20 × 20 subapertures. This figure shows that high-order modes are the first to be affected by

★ E-mail: cheritie@eso.org

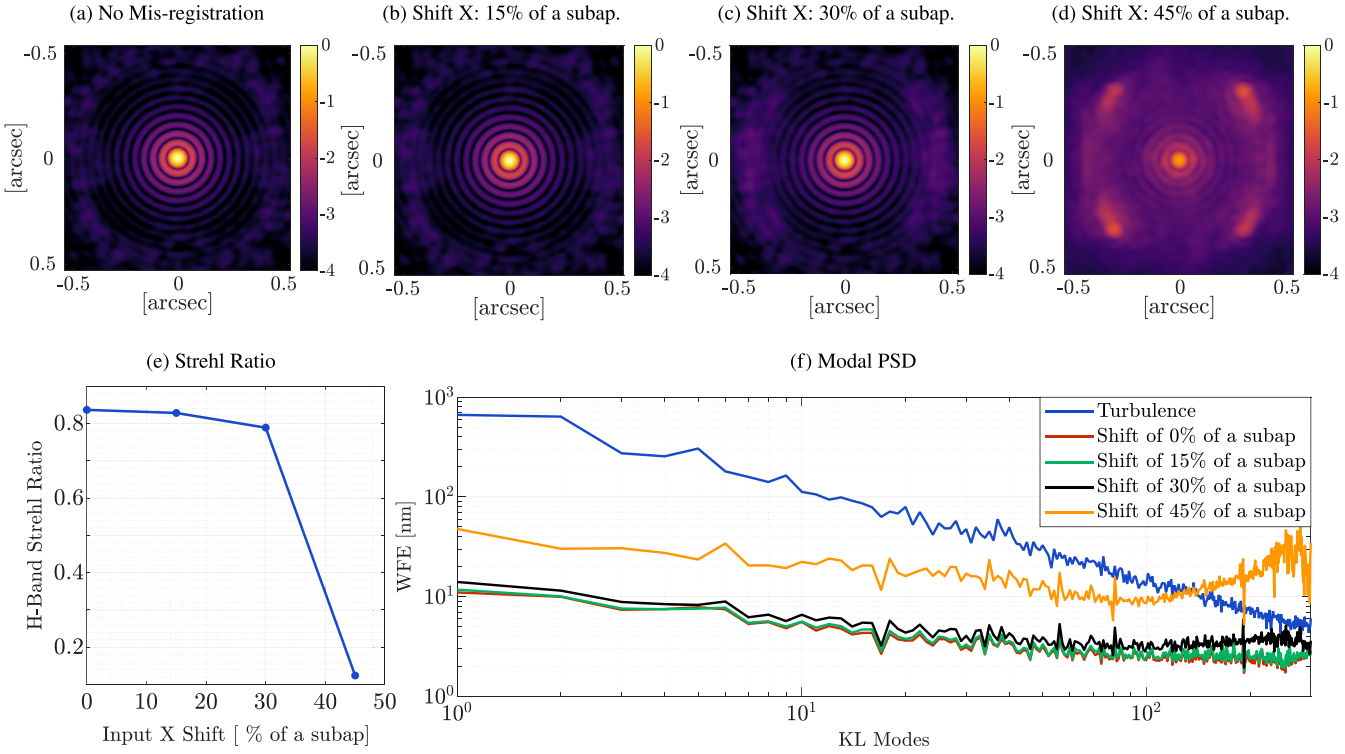

Figure 1. Effect of a mis-registration on the performance of an 8-m class telescope equipped with a 20 × 20 sub-apertures AO system. Top: effect of a shift on the *H*-band PSF. Bottom: effect of a shift on the AO performance, where SR denotes the Strehl ratio and PSD is the modal PSD.

the mis-registrations. This is visible in the PSFs (Figs 1a and 1b), which exhibit speckles on the external rings of the Airy pattern, and in the modal power spectral density (PSD) of the AO residuals (Fig. 1d), which exhibits peaks going above the turbulence level for the high-order modes. For large values of shift (above 30 per cent of a subaperture), the loop becomes even unstable (Fig. 1 b and 1c) and would require interruption of the scientific operation to recalibrate the system.

Hence, to provide a nominal correction for the scientific instruments, the AO loop has to be properly calibrated before and during the operations. The accuracy required for the WFS/DM registration to prevent any effect on the scientific operation is system-dependent and depends on the number of modes controlled by the AO loop. The value of 10 per cent of a subaperture shift (and equivalent shift on the border of the pupil for the rotation) is usually taken as a reference (Béchet, Tallon & Thiébaut 2012; Heritier et al. 2018b) but should be carefully evaluated (see Section 4.5).

In this context, a scheme based on the use of pseudo-synthetic models to calibrate the AO systems has been proposed (Oberti et al. 2006; Béchet et al. 2012; Kolb et al. 2012; Heritier et al. 2018a, 2018b). It offers a fast way to numerically update the calibration of the system and relies only on the identification of a few model mis-registration parameters. By contrast, a scheme where the calibration is achieved using only on-sky measurements (Pinna et al. 2012) would require long telescope overheads (see Section 2.2). A pseudo-synthetic calibration is necessary to develop a synthetic model that must be representative of the real AO system to allow us to compute its associated interaction matrix numerically (equation 1). A block diagram summarizing the principle of a pseudo-synthetic calibration is provided in Fig. 2. It shows the following key elements of the model.

(i) The synthetic model is usually developed using an end-to-end simulator. It includes the DM and WFS and the corresponding sensitivity to the different mis-registrations. In this paper, we use the OOMAO simulator (Conan & Correia 2014) that has been validated at the Large Binocular Telescope (LBT; Heritier et al. 2018b).

(ii) Experimental inputs are used to tune the model, such as WFS valid pixels, DM influence functions, modal basis, WFS signals, etc.

(iii) A mis-registration identification algorithm is fed on experimental inputs (DM commands and WFS signals that are representative of the real mis-registration $\boldsymbol{\alpha}$). In this paper, the strategy consists of projecting a given experimental signal that is composed of on-sky measurements of a few well-selected modes on to sensitivity interaction matrices that correspond to these modes. More details can be found in Section 3.1.

This paper focuses on the identification of the mis-registration parameters but more information about synthetic modelling of real AO systems can be found in Oberti et al. (2006), Pinna et al. (2012), Kolb et al. (2012) and Heritier et al. (2018b).

Previous research works have already investigated the tracking of mis-registration parameters. For instance, at the Adaptive Optics Facility (AOF; Arsenault et al. 2008), the calibration baseline is to use a pseudo-synthetic model in which mis-registration parameters are identified from closed-loop data (Béchet et al. 2011; Kolb et al. 2012; Oberti et al. 2018). This identification strategy consists of correlating the incremental closed-loop DM commands to the incremental WFS signals to capture the interaction between the WFS and DM. In Neichel et al. (2012), a strategy based on a Levenberg–Marquardt (Marquardt 1963) type algorithm is presented in the frame of tomographic AO systems but requires an experimental interaction matrix as a reference, which could for instance be measured on-

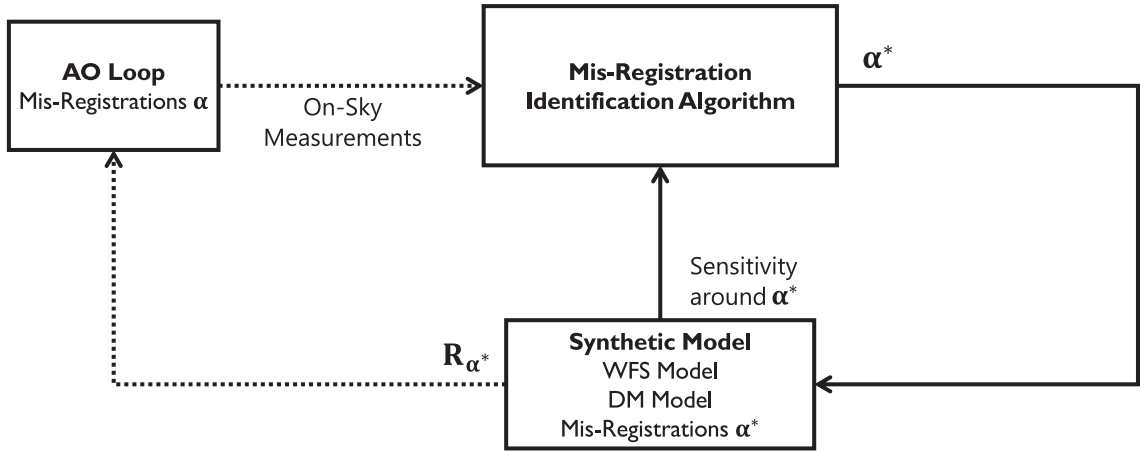

Figure 2. Principle of the pseudo-synthetic calibration. Experimental inputs representative of the real mis-registration state $\boldsymbol{\alpha}$ are injected into a mis-registration identification algorithm that provides an estimation $\boldsymbol{\alpha}^*$. The identification algorithm is presented in Section 3.1.

sky. In the frame of multi-conjugate AO systems, the identification of the interaction matrix using on-sky signals has been investigated in Chiuso, Muradore & Marchetti (2010). More recently, Lai et al. (2021) have studied ground-layer AO systems, using a model-free method to reconstruct fully the interaction matrix injecting known random signals on the DM during the operation.

In this paper, we present a new strategy to monitor the mis-registrations during the operations by applying known (and invisible to the science in most of the cases) perturbations on the DM and to update the calibration using synthetic models of the AO systems. In particular, we investigate whether the perturbation can be reduced to only a few well-selected modes to provide a good estimation of the mis-registration parameters and to minimize the effect on the science path to make it compatible with single-conjugate AO applications.

For the sake of simplicity, we consider in this paper a simple AO system with 20 × 20 subapertures and an 8-m class telescope to properly validate and characterize the method. In addition, the experience acquired at the AOF showed that magnifications X and Y were initially measured but eventually removed from the tracked parameters as they appeared to remain static over time. For this reason, we reduce the study to the tracking of only three mis-registration parameters (shifts X and Y, and rotation) as being the most occurring mis-registration errors (due to mechanical flexures and de-rotation errors). If required, the structure of the mis-registration identification algorithm (Section 3.1) is fully compatible with any other type of mis-registration. It is then straightforward to include other types of mis-registrations depending on the system considered.

The performance of the method for an ELT-like system will be investigated in a second step to include more complex challenges that will affect the closed-loop operations (Bonnet et al. 2018; Le Louarn et al. 2016), in particular in presence of variations of large optical gains when operating with a PWFS (Deo et al. 2018, 2019b; Chambouleyron et al. 2020), pupil fragmentation effects due to the large thickness of the spiders holding the secondary mirror (Bonnefond et al. 2016; Schwartz et al. 2018; Bertrou-Cantou et al. 2020), the effect of phasing errors for segmented primary mirrors (Meimon et al. 2008; Briguglio et al. 2018b; Cheffot et al. 2020) and complex and large adaptive secondary mirrors (Biasi et al. 2010; Riccardi et al. 2010; Madec 2012; Vernet et al. 2014; Briguglio et al. 2018a).

We first recall the AO calibration procedures for post-focal AO systems and large adaptive telescopes in Section 2. The strategy to monitor the mis-registrations using on-sky measurements is presented in Section 3 and an analysis of the accuracy and robustness of the method is provided in Section 4, as well as an analysis of the effect on the scientific path.

2 CALIBRATION OF AN AO SYSTEM

The interaction matrix $\mathbf{D}_{\boldsymbol{\alpha}}$ of an AO system is defined as the image of the DM influence functions $\mathbf{M}_{\mathrm{DM}_{\boldsymbol{\alpha}}}$ as seen by the WFS,

$$\mathbf{D}_{\boldsymbol{\alpha}} = \mathbf{M}_{\mathrm{WFS}} \cdot \mathbf{M}_{\mathrm{DM}_{\boldsymbol{\alpha}}}, \tag{1}$$

where $\mathbf{M}_{\mathrm{WFS}}$ is the WFS measurement model and the notation $\boldsymbol{\alpha}$ corresponds to the DM/WFS registration state. The notations chosen here correspond to apply the mis-registrations in the DM space, considering that the WFS is fixed. In addition, we assume that the image of the pupil remains fixed on the WFS and that there are no errors of pupil stabilization. To operate the AO system in a closed loop, it is necessary to invert the interaction matrix to provide the command matrix $\mathbf{R}_{\boldsymbol{\alpha}}$. This is often achieved using a truncated singular value decomposition (TSVD), removing the modes associated with the lowest singular values (Boyer, Michau & Rousset 1990). More advanced inversion methods such as adding priors on the noise and turbulence allows us to improve the level of AO correction (Wallner 1983; Fusco et al. 2001).

The interaction matrix of the system is usually projected on to a reduced modal basis, which differs from the zonal actuation and contains only the modes well seen by the WFS. This allows us to preliminary filter out the modes badly seen by the AO system and it provides a stable inversion of the interaction matrix. Typically, a common method is to use Karhunen–Loèves (KL) modes that are computed by diagonalizing both the statistical covariance matrix of the atmosphere and the geometrical covariance matrix of the DM influence functions (Gendron 1995). In this paper, the closed-loop control is always done using a number of KL modes slightly inferior to the number of actuators located in the pupil, to ensure a small conditioning number for the interaction matrix (inferior to 10) and thus a stable inversion.

2.1 Interaction matrix estimation of a post-focal AO system

For a post-focal AO system, the interaction matrix is usually estimated prior to the operations using a set of calibration signals $\mathbf{U}$

that defines the control space of the AO loop, such as the KL modes introduced above. In the following, it is however assumed that the matrix **U** is full rank, which corresponds to calibrating all the degrees of freedom of the DM. The WFS measurements **Y** corresponding to the actuation signals **U** are given by

$$\mathbf{Y} = \mathbf{M}_{\mathrm{WFS}} \cdot [\mathbf{M}_{\mathrm{DM}_{\boldsymbol{\alpha}}} \cdot \mathbf{U} + \boldsymbol{\Phi}] + \eta, \tag{2}$$

where Φ is the local turbulence and η is the WFS noise (photon and readout noise).

Assuming that both the amplitude of the calibration signals and the local turbulence are small enough to remain in the linear regime of the WFS, the previous equation can be distributed such that the interaction matrix $\mathbf{D}_{\boldsymbol{\alpha}}$ of the system appears (equation 1)

$$\mathbf{Y} = \mathbf{D}_{\boldsymbol{\alpha}} \cdot \mathbf{U} + \mathbf{M}_{\mathrm{WFS}} \cdot \boldsymbol{\Phi} + \eta. \tag{3}$$

The interaction matrix of the system can be estimated by computing

$$\mathbf{D}_{\boldsymbol{\alpha}} = \mathbf{Y} \cdot \mathbf{U}^{\dagger} - [\mathbf{M}_{\mathrm{WFS}} \cdot \boldsymbol{\Phi} + \eta] \cdot \mathbf{U}^{\dagger}, \tag{4}$$

where $[\mathbf{M}_{\mathrm{WFS}} \cdot \boldsymbol{\Phi} + \eta] \cdot \mathbf{U}^{\dagger}$ is the calibration error on the interaction matrix estimation and the symbol † represents the pseudo-inverse.

For a post-focal AO system, where both the DM and WFS are located on the same bench, the local turbulence can be considered as negligible and the use of a bright external calibration source allows us to minimize the contribution of the measurement noise η so that

$$\mathbf{D}_{\boldsymbol{\alpha}} = \mathbf{Y} \cdot \mathbf{U}^{\dagger}. \tag{5}$$

In this situation, the evolution of the mis-registrations is slow as both the DM and WFS are located on the same optical bench. The validity of $\mathbf{D}_{\boldsymbol{\alpha}}$ is then granted for a long period of time and can easily be recalibrated using day-time calibration, plugging an external calibration source.

2.2 Calibration of an AO system for large adaptive telescopes

In the case of adaptive telescopes, frequent evolution of the DM/WFS registration is to be expected due to flexures and to the large distance separating the DM from the AO instrument. In addition, the access to an external calibration source is not often granted, which leads to a consideration of different approaches to calibrate the AO system.

Regarding the first point, to provide nominal AO performance, it becomes necessary to regularly monitor and compensate for the mis-registrations during the operations. Considering the situation in which an AO system has been calibrated in a registration state α_0 and evolved to a registration state α, the compensation of the mis-registrations can be achieved following two strategies.

(i) The compensation can be achieved by updating the interaction matrix corresponding to the new DM/WFS registration. Using the notations introduced in this paper, it corresponds to the following transformation:

$$\mathbf{D}_{\boldsymbol{\alpha}_0} \rightarrow \mathbf{D}_{\boldsymbol{\alpha}}. \tag{6}$$

(ii) The compensation can be done optically, by physically re-aligning some elements in the optical path. This corresponds to the following transformation:

$$\mathbf{M}_{\mathrm{DM}_{\boldsymbol{\alpha}}} \rightarrow \mathbf{M}_{\mathrm{DM}_{\boldsymbol{\alpha}_0}}. \tag{7}$$

The update of the interaction matrix can be obtained experimentally by measuring a full interaction matrix during the operation (Oberti et al. 2004, 2006; Pinna et al. 2012) or by computing the new interaction matrix numerically from a pseudo-synthetic model, fed with a few experimental parameters (Oberti et al. 2004, 2018; Kolb et al. 2012; Béchet et al. 2012; Heritier et al. 2018b).

Thus, in the context of the future large adaptive telescopes, fast evolution of potentially large mis-registrations is expected. Achieving a full measurement of the interaction matrix at each update comes then with a cost in terms of telescope operation, in particular with such a large number of degrees of freedom to calibrate (typically around 5000 modes; Vernet et al. 2012) in the case of the ESO ELT. The corresponding time required to obtain high signal-to-noise ratio (S/N) measurements of the interaction matrix becomes problematic especially because its validity is only ensured at the time of the measurement. Typically, for the de-commissioned FLAO system at the LBT, a full measurement of the on-sky interaction matrix, multiplexing two modes at the same time, required 53 min of telescope time (including overheads; Pinna et al. 2012). Extrapolating these numbers to an ELT SCAO system (which contains about 10 times more degrees of freedom) leads to potentially several hours of calibration time, during which the measurements could be affected by mis-registrations and eventual optical gains variations in the case of a PWFS (Korkiakoski, Vérinaud & Le Louarn 2008; Deo et al. 2018, 2019a; Chambouleyron et al. 2020).

As a consequence, in this context, this strategy does not seem suited to provide a regular tracking of the calibration during the operations. However, the method could be useful at the beginning of the observations to provide a first interaction matrix that would be used as a reference for the next steps of calibration or to measure only a few reference signals and retrieve mis-registration parameters (see Section 3).

To comply with these requirements of fast and regular updates, a calibration based on the on-sky identification of few mis-registration parameters, making use of a synthetic model of the interaction matrix, appears to be a good candidate as it allows us either to recompute a whole interaction matrix (which will also have the advantage of being noise-free) or to realign physically the optical system.

Updating the full interaction matrix $\mathbf{D}_{\boldsymbol{\alpha}}$ numerically (equation 6) provides the easiest solution in terms of software architecture as the only output is a reconstructor $\mathbf{R}_{\boldsymbol{\alpha}}$ that is injected into the RTC. It requires a tuning of the model that can be achieved during the commissioning phase of the instrument using experimental measurements of the real system. In addition, it also allows us to include high-order mis-registrations such as distortion that might not be correctable with an optical device. However, if too large mis-registrations occur, the AO performance could be affected due to an unusual DM/WFS registration. For instance, in a Fried geometry, locating the actuators of a system in the centre of the WFS subapertures could result in a loss of sensitivity (Southwell 1980) depending on the AO system properties (actuator mechanical coupling and WFS subaperture size and number). In addition, depending on the optical design of the system, large drifts of the system could lead to pupil truncation effects, DM actuators not seen by the WFS subapertures and/or WFS subapertures corresponding to non-controlled actuators. All of these things will affect the performance of the AO system.

Alternatively, the second compensation strategy allows us to optically realign the system (equation 7) and ensures that it always operates around the nominal working point (i.e. keeping the DM/WFS registration constant around the optimal configuration). In that case, the computation of only one numerical interaction matrix is required, which reduces the computational load of the approach. However, it requires a more complex software architecture to control opto-mechanical elements in the optical path that are more limited in terms of degrees of freedom than a numerical model.

The choice of the compensation strategy is system-dependent and might be driven by other constraints in terms of software or hardware configuration. Thus, we focus only on the identification of the mis-registration parameters and we do not investigate the AO performance when a given type of compensation is applied. In addition, it is assumed that the model of the system has been perfectly tuned to be representative of the real system considered. Therefore, the results presented do not include model errors other than mis-registration estimation errors.

3 MIS-REGISTRATION IDENTIFICATION STRATEGY

In this section, we introduce a strategy that consists of acquiring on-sky signals to identify the mis-registration parameters. The particularity of this approach is that it can be applied either offline or during operation. In the latter case, it shall be verified that the actual effect on the science observations can be neglected, as the signals could act as a noise on the scientific measurements depending on the signal amplitude.

The strategy to acquire the signals required by the mis-registration identification algorithm is based on the same methods used for on-sky calibrations: dithering specific signals over the closed-loop DM commands using either fast push–pull measurements or sinusoidal modulation. More details about on-sky calibration can be found in Oberti et al. (2004, 2006), Pieralli et al. (2008) and Pinna et al. (2012).

If the acquisition has to be achieved during the operation, a scheme based on a sinusoidal modulation of the signals seems better suited as it allows us to reduce the amplitude of the dithering signals to reach the same S/N obtained using a push–pull approach, hence reducing the effect on the science. However, this requires a good knowledge of the AO loop properties, in particular the loop delay (Pinna et al. 2012). For both methods, the S/N of the on-sky acquisition depends on the observing conditions (turbulence, level of noise) and on the AO system properties (number of actuators, bandwidth). The parameters for the signal measurements such as duration, frequency of modulation and amplitude of the signals have then to be tailored accordingly. Because both methods allow us to retrieve signals with equivalent S/N, we propose to consider only the push–pull measurements to narrow down the analysis to the spatial properties of the signals. Some examples of the effect of the temporal modulation of signals on the science path are available in Deo et al. (2019b) and Esposito et al. (2020). In this section, we detail the three key steps of the identification strategy: the mis-registration identification algorithm (Section 3.1), the closed-loop signal acquisition strategy (Section 3.2) and the choice of the signal (Section 3.3).

3.1 Mis-registration identification algorithm

3.1.1 Principle

We describe the principle of the mis-registration identification algorithm to extract the mis-registration parameters from a given interaction matrix that can be projected on a given modal basis. This algorithm is based on the work presented in Kolb et al. (2012) but we have adapted it to take into consideration the PWFS optical gains and only a small number of signals from the interaction matrix. The general idea is to project an estimation of the interaction matrix on a set of sensitivity matrices that describe the sensitivity of the system to a given type of mis-registration around a given working point (in a small perturbation regime). This is based on the hypothesis that a given interaction matrix $\mathbf{D}_{\boldsymbol{\alpha}}$ can be decomposed as a linear combination of sensitivity matrices around the working point $\boldsymbol{\alpha}_0$:

$$\mathbf{D}_{\boldsymbol{\alpha}} = \mathbf{G}\left[\mathbf{D}_{\boldsymbol{\alpha}_0} + \sum_i \alpha_i \cdot \delta\mathbf{D}_{\boldsymbol{\alpha}_0}(\varepsilon_i)\right]. \tag{8}$$

Here, $\mathbf{G}$ is a diagonal matrix accounting for the gain variations between $\mathbf{D}_{\boldsymbol{\alpha}}$ and $\mathbf{D}_{\boldsymbol{\alpha}_0}$. The origin of these gain variations is the mis-registrations and the fact that $\mathbf{D}_{\boldsymbol{\alpha}}$ can be acquired on-sky and exhibits optical gains variations, as is the case for PWFS.[1] The sensitivity matrices $\boldsymbol{\delta}\mathbf{D}_{\boldsymbol{\alpha}_0}(\varepsilon_i)$ are defined as the partial directional derivative of the interaction matrix corresponding to a mis-registration of type i (typically rotation and shifts):

$$\boldsymbol{\delta}\mathbf{D}_{\boldsymbol{\alpha}_0}(\varepsilon_i) = \left[\frac{\mathbf{D}(\boldsymbol{\alpha}_0 + \varepsilon_i) - \mathbf{D}(\boldsymbol{\alpha}_0 - \varepsilon_i)}{2\varepsilon_i}\right]_{i=rot,X,Y,\ldots}. \tag{9}$$

Here, $\boldsymbol{\alpha}_0$ is the working point of the system or, in other words, the vector of mis-registration amplitudes corresponding to the alignment of the system at this operating point, and ε_i is a vector of mis-registration amplitudes to compute the sensitivity matrices, chosen to be small enough to remain in the domain of validity of the hypothesis of linearity (typically 1 per cent of the subaperture). The notation ε_i corresponds to the small mis-registration applied to compute the interaction matrix and is different from the parameter $\boldsymbol{\alpha}_i$ that corresponds to the mis-registration to identify.

For each type of mis-registration, the corresponding sensitivity matrices are concatenated in a meta sensitivity matrix $\boldsymbol{\Lambda}_{\boldsymbol{\alpha}_0}$[2]

$$\boldsymbol{\Lambda}_{\boldsymbol{\alpha}_0} = \left[\boldsymbol{\delta}\mathbf{D}_{\boldsymbol{\alpha}_0}(\varepsilon_{\text{rot}})\ \boldsymbol{\delta}\mathbf{D}_{\boldsymbol{\alpha}_0}(\varepsilon_X)\ \boldsymbol{\delta}\mathbf{D}_{\boldsymbol{\alpha}_0}(\varepsilon_Y)\ \ldots\right] \tag{10}$$

such that equation (8) can be rewritten as

$$\mathbf{D}_{\boldsymbol{\alpha}} = \mathbf{G}\left(\mathbf{D}_{\boldsymbol{\alpha}_0} + \boldsymbol{\alpha} \cdot \boldsymbol{\Lambda}_{\boldsymbol{\alpha}_0}\right) \tag{11}$$

where $\boldsymbol{\alpha}$ is the vector of mis-registration parameters defined as

$$\boldsymbol{\alpha} = \begin{Bmatrix} \alpha_{\text{rot}} \\ \alpha_X \\ \alpha_Y \\ \ldots \end{Bmatrix}. \tag{12}$$

The goal is to identify $\boldsymbol{\alpha}^*$ that minimizes the criterion:

$$\boldsymbol{\alpha}^* = \arg\min_{\mathbf{G},\boldsymbol{\alpha}} \left\|\mathbf{D}_{\boldsymbol{\alpha}} - \mathbf{G}\left(\mathbf{D}_{\boldsymbol{\alpha}_0} + \boldsymbol{\alpha} \cdot \boldsymbol{\Lambda}_{\boldsymbol{\alpha}_0}\right)\right\|^2. \tag{13}$$

The convergence conditions of the criterion are discussed in Section 3.1.3. The solution of the least-squares criterion is given by

$$\mathbf{G}^* = \text{diag}\left[(\mathbf{D}_{\boldsymbol{\alpha}_0} + \boldsymbol{\alpha}^* \boldsymbol{\Lambda}_{\boldsymbol{\alpha}_0})^\dagger \cdot \mathbf{D}_{\boldsymbol{\alpha}}\right] \tag{14}$$

and

$$\boldsymbol{\alpha}^* = (\boldsymbol{\Lambda}_{\boldsymbol{\alpha}_0})^\dagger \cdot \left(\mathbf{D}_{\boldsymbol{\alpha}\mathbf{G}^*}^{-1} - \mathbf{D}_{\boldsymbol{\alpha}_0}\right). \tag{15}$$

3.1.2 Implementation

Because it is necessary to identify both $\mathbf{G}^*$ and $\boldsymbol{\alpha}^*$, the algorithm has to be iterative. One iteration of the algorithm has two steps. The first step is to estimate the optical gains taking $\boldsymbol{\alpha}^* = \mathbf{0}$ as a starting point, by rewriting equation (14):

$$\mathbf{G}_1^* = \text{diag}\left(\mathbf{D}_{\boldsymbol{\alpha}_0}^\dagger \cdot \mathbf{D}_{\boldsymbol{\alpha}}\right). \tag{16}$$

[1] This is based on the hypothesis that the optical gains matrix can be considered as diagonal (Deo et al. 2018; Chambouleyron et al. 2020)

[2] In practice, the matrices $\boldsymbol{\delta}\mathbf{D}_{\boldsymbol{\alpha}_0}(\varepsilon_i)$ are reshaped as vectors $\boldsymbol{\delta}\mathbf{d}_{\boldsymbol{\alpha}_0}(\varepsilon_i)$, of length $N_S = N_{\text{WFS}}$ WFS signals $\times$ N_{DM} sets of DM commands, but for the sake of clarity, we prefer the matrix notation.

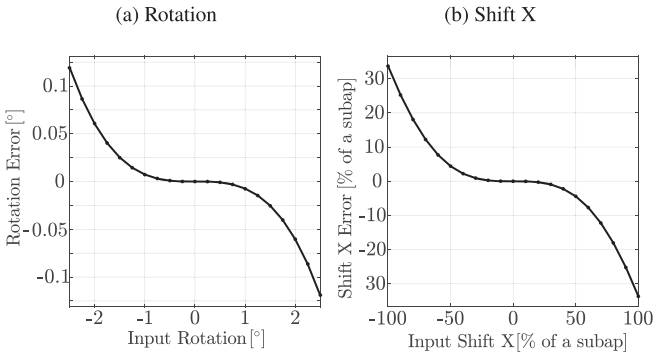

Figure 3. Linearity curves of the identification algorithm for the rotation (left) and shift *X* (right).

The value of $\mathbf{G}_1^*$ is inserted into equation (15) to obtain the first estimation of $\boldsymbol{\alpha}^*$:

$$\boldsymbol{\alpha}_1^* = (\boldsymbol{\Lambda}_{\boldsymbol{\alpha}_0})^\dagger \cdot (\mathbf{D}_{\boldsymbol{\alpha}} \mathbf{G}_1^{*\,-1} - \mathbf{D}_{\boldsymbol{\alpha}_0}). \tag{17}$$

From the estimation $\boldsymbol{\alpha}_1^*$, the matrix $\mathbf{D}_{\boldsymbol{\alpha}_0}$ can be updated by computing the new interaction matrix $\mathbf{D}_{\boldsymbol{\alpha}_1^*}$ corresponding to the mis-registration $\boldsymbol{\alpha}_1^*$ and finding the next estimation of $\mathbf{G}_2^*$ using equation (14). In practice, only a few iterations are required to converge. In our case, we consider that the algorithm has converged once the relative error between two successive estimations of the parameters is under 1 per cent.

3.1.3 Convergence conditions

The criterion defined in equation (13) is derived from the first-order Taylor development of the interaction matrix (equation 8). By construction, its convexity and the uniqueness of the solution are only ensured within a limited linear range. We did not formally investigate the convergence limitations of the procedure but it has been verified that the algorithm converges for a large range of values around the operating point (up to 70 per cent of a subaperture shift and more than 2° of rotation).

As a complement, we provide the linearity curves for both rotation and shift parameters in Fig. 3. These plots show that within 60 per cent of a subaperture shift and within 1°.5 of rotation, the algorithm remains very linear. For larger mis-registrations, the working point $\boldsymbol{\alpha}_0$ around which the sensitivity matrices are computed must be updated. This is achieved by computing $\boldsymbol{\Lambda}_{\boldsymbol{\alpha}^*}$ after each estimation[3] or by physically realigning the system after each estimation. This will allow the algorithm to converge to the right parameters using only a few iterations. Using this iterative approach, it has been empirically verified that the algorithm converges for very large mis-registrations (5° of rotation and more than 100 per cent of a subaperture shift).

If the mis-registrations are too far out of the linear regime, typically 300 per cent of a subaperture shift or 20° of rotation, the convergence of the algorithm is no longer granted. In addition, for such large mis-alignments, depending on the optical design, pupil truncation effects could alter the convergence of the algorithm; however, this topic is out of the scope of this paper. These very large mis-registrations should only occur during the commissioning phase where other less accurate methods could be used, for instance based on flux considerations, and could provide a rough estimate of the mis-registration parameters.

[3]The estimation of $\boldsymbol{\alpha}^*$ is the convergence value of the iterative procedure to identify both scaling factors $\mathbf{G}^*$ and mis-registration parameters $\boldsymbol{\alpha}^*$.

In closed-loop conditions, the system is not expected to drift too far from its initial working point, at least not on a fast time-scale, and no problem of convergence is expected.

3.2 On-sky push–pull measurement

In the previous section, we presented the procedure to identify mis-registration parameters from a given interaction matrix. Here, we now recall how to calibrate on-sky an interaction matrix, or a subset of it. The measurement $\mathbf{y}_k$ of the WFS at the loop sample k is given by

$$\mathbf{y}_k = \mathbf{M}_{\mathrm{WFS}} \cdot \boldsymbol{\phi}_k^{\mathrm{res}} + \boldsymbol{\eta}_k, \tag{18}$$

where $\mathbf{M}_{\mathrm{WFS}}$ defines the WFS measurement model (see equation 1). The push–pull measurement of a mode, represented by a phase vector $\boldsymbol{b}$, requires

$$\mathbf{y}_k^{+b} = \mathbf{M}_{\mathrm{WFS}} \cdot \boldsymbol{\phi}_k^{\mathrm{res}} + \boldsymbol{\eta}_k + a \cdot \mathbf{M}_{\mathrm{WFS}} \cdot \boldsymbol{b} \tag{19}$$

and

$$\mathbf{y}_k^{-b} = \mathbf{M}_{\mathrm{WFS}} \cdot \boldsymbol{\phi}_{k+1}^{\mathrm{res}} + \boldsymbol{\eta}_{k+1} - a\mathbf{M}_{\mathrm{WFS}} \cdot \boldsymbol{b}, \tag{20}$$

where a is the amplitude of the mode considered. The sensitivity measurement $\mathbf{y}_k^{\boldsymbol{b}}$ of the mode $\boldsymbol{b}$ is then given by

$$\begin{aligned}\mathbf{y}_k^{\boldsymbol{b}} &= \frac{\mathbf{y}_k^{+\boldsymbol{b}} - \mathbf{y}_k^{-\boldsymbol{b}}}{2a} \\ &= \mathbf{M}_{\mathrm{WFS}} \cdot \boldsymbol{b} + \frac{\mathbf{M}_{\mathrm{WFS}} \cdot (\boldsymbol{\phi}_k^{\mathrm{res}} - \boldsymbol{\phi}_{k+1}^{\mathrm{res}}) + \boldsymbol{\eta}_k - \boldsymbol{\eta}_{k+1}}{2a}.\end{aligned} \tag{21}$$

We can define the disturbance terms as

$$\boldsymbol{\xi}_k = \frac{-\mathbf{M}_{\mathrm{WFS}} \cdot \boldsymbol{\delta\phi}_k^{\mathrm{res}} + \boldsymbol{\eta}_k - \boldsymbol{\eta}_{k+1}}{2a}, \tag{22}$$

where we define the incremental residual turbulence $\boldsymbol{\delta\phi}_k^{\mathrm{res}}$ as

$$\boldsymbol{\delta\phi}_k^{\mathrm{res}} = \boldsymbol{\phi}_{k+1}^{\mathrm{res}} - \boldsymbol{\phi}_k^{\mathrm{res}}. \tag{23}$$

The push–pull measurement $\mathbf{y}_k^{\boldsymbol{b}}$ is then given by

$$\mathbf{y}_k^{\boldsymbol{b}} = \mathbf{M}_{\mathrm{WFS}} \cdot \boldsymbol{b} + \boldsymbol{\xi}_k. \tag{24}$$

In practice, to improve the S/N of the measurement, we average N push–pull measurements to estimate $\overline{\mathbf{y}^{\boldsymbol{b}}}$:

$$\overline{\mathbf{y}^{\boldsymbol{b}}} = \frac{1}{N}\sum_k^N \mathbf{y}_k^{\boldsymbol{b}} = \mathbf{M}_{\mathrm{WFS}} \cdot \boldsymbol{b} + \frac{1}{N}\sum_k^N \boldsymbol{\xi}_k. \tag{25}$$

The composition of $\boldsymbol{\xi}_k$ shows that the S/N of $\overline{\mathbf{y}^{\boldsymbol{b}}}$ will depend on the level of noise $\boldsymbol{\eta}_k$, the amplitude of the signal a, the difference between two successive residual phases $\boldsymbol{\delta\phi}_k^{\mathrm{res}}$ and the number of measurements N averaged. The accuracy of the estimation of the mis-registration parameters will then depend on the brightness of the source (noise level), the amplitude of the modulation and the quality of the AO correction.

3.3 An optimal modal basis for the mis-registration identification?

One important goal of this research is to make the calibration invisible to the science path while being as fast as possible. For this purpose, we propose to identify the most sensitive modes to a given mis-registration and thus to minimize the number of signals required to extract the mis-registration parameters. This will particularly be relevant for ELT AO instruments, as the acquisition of an on-sky interaction matrix corresponding to several thousands of modes will

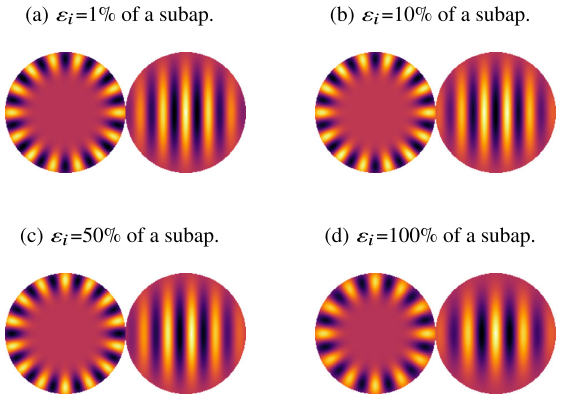

Figure 4. Most sensitive mode corresponding to the rotation (left) and the shift X (right) derived from the PCA of $\boldsymbol{\delta}\mathbf{D}_{\boldsymbol{\alpha}_0}(\varepsilon_i)$ for different values of $\varepsilon_i = 1$ per cent.

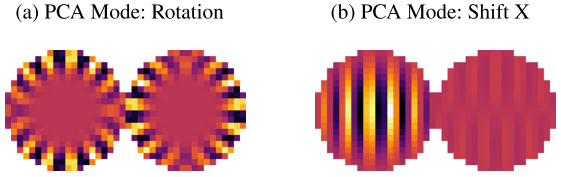

Figure 5. WFS measurement [slope X, slope Y] corresponding to the most sensitive modes for the rotation (a) and the shift X (b). In this example, $\varepsilon_i = 1$ per cent of a subaperture (Fig. 4a).

require long measurement time, leading to large overheads and thus reducing significantly the time available for the scientific operation.

To do so, we propose to apply a principal component analysis (PCA; Pearson 1901) on a sensitivity matrix $\boldsymbol{\delta}\mathbf{D}_{\boldsymbol{\alpha}_0}(\varepsilon_i)$, which is defined as the derivative of the interaction matrix with respect to a mis-registration of type i (see equation 9). A similar approach was proposed by Oberti et al. (2018) but was based on flux considerations.

We proceed to the singular value decomposition (SVD) of $\boldsymbol{\delta}\mathbf{D}_{\boldsymbol{\alpha}_0}(\varepsilon_i)$,[4] which contains the measurement for the $N_{\rm DM}$ degrees of freedom of the DM (a zonal interaction matrix, for instance):

$$\boldsymbol{\delta}\mathbf{D}_{\boldsymbol{\alpha}_0}(\varepsilon_i) = \mathbf{U}\cdot\mathbf{S}\cdot\mathbf{V}^{\rm T}. \tag{26}$$

By definition, the variance contained in the signals of $\boldsymbol{\delta}\mathbf{D}_{\boldsymbol{\alpha}_0}(\varepsilon_i)$ and due to the input mis-registration ε_i is given by λ_i,

$$\lambda_i = \frac{1}{N_{\rm DM}} s_i^2, \tag{27}$$

where s_i is the ith singular value of $\boldsymbol{\delta}\mathbf{D}_{\boldsymbol{\alpha}_0}(\varepsilon_i)$ and thus the ith element of the diagonal matrix $\mathbf{S}$.

By construction, the first singular modes $\mathbf{v}$ of $\mathbf{V}$ contain most of the variance due to the perturbation injected (the mis-registration ε_i). An illustration of these PCA modes is given in Fig. 4, displaying the most sensitive modes to the rotation and shift X for different values of ε_i (for the rotation, the value represents the equivalent shift for the actuators located at the edge of the pupil). The corresponding WFS measurement is given in Fig. 5.

[4]To apply the PCA, the mean value of each mode measurement (i.e. a row of the sensitivity matrix) has to be subtracted to provide mean centred sensitivity matrices.

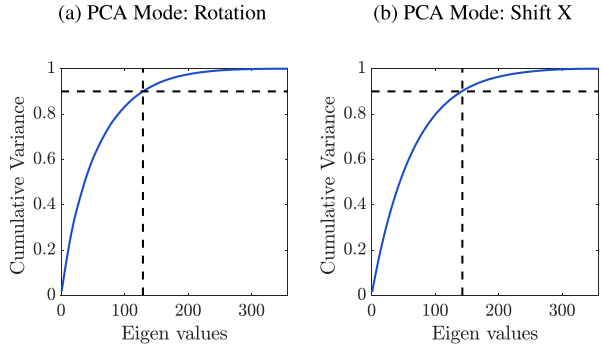

Figure 6. Normalized cumulative variance corresponding to the rotation (a) and shift X (b). In this example, $\varepsilon_i = 1$ per cent of a subaperture (Fig. 4a).

The modes of Fig. 4 are consistent with what one would expect: a radial non-symmetry with the signal localized on the edge of the pupil for the rotation and a Fourier-like mode for the shift. We notice that the spatial frequency of the modes is actually quite low; we would have expected higher spatial frequencies considering that there are 20 actuators along one diameter. However, this also depends on the WFS geometry. It appears that using significantly larger values of mis-registrations has a small effect on the spatial frequency of the PCA modes. Changes start to be visible when ε_i is above 50 per cent of a subaperture shift, with PCA modes exhibiting a slightly lower spatial frequency (Fig. 4c). This result suggests that one single set of modes could be pre-computed and kept for both types of application: closed-loop operations that require a fine tuning of the parameters (as the mis-registrations should remain small enough to allow a stable closed loop) and commissioning of an instrument where the mis-registrations to identify might be much larger.

Fig. 6 gives the cumulative variance associated with the PCA modes. This figure shows some important information; more than 100 PCA modes are required to explain 90 per cent of the variance due to a mis-registration in all cases. This shows that the reduction of dimensionality is not so efficient. In other words, this means that the sensitivity of the first PCA mode and any other of the 100 first PCA modes will be similar. This gives some flexibility in the choice of the mode to use and other criteria that are system-dependent might also be considered.

The advantage of this procedure remains that it clearly identifies a single mode per mis-registration that takes into consideration the AO system sensitivity according to the DM and WFS geometry, DM mechanical coupling and maximum stroke and WFS sampling and sensitivity. Moreover, the procedure is very general and can be used to define PCA modes for other types of mis-registrations that were not considered in this study (the anamorphosis or distortion, for instance). It will be relevant to investigate how the method performs for these higher-order mis-registrations and if coupling between the mis-registration parameters appear, typically between a magnification in X and a shift X (Chambouleyron et al. 2020).

4 APPLICATION: NUMERICAL SIMULATIONS

In this section, we investigate the feasibility of tracking mis-registration parameters using the strategy presented in Section 3, using end-to-end simulations in the OOMAO simulator (Conan & Correia 2014). We propose to explore different closed-loop conditions of noise and turbulence as discussed in Section 3.2, simulating a simple AO system whose properties are summarized in Table 1. In the analysis, we considered both a PWFS (Ragazzoni

Table 1. Parameters of the numerical simulations.

Turbulence	Fried parameter r_0	8–15 cm @550 nm
	Outer scale L_0	30 m
	Cn^2 profile	One layer
	Wind speed	10–30 m s^{-1}
Control	Frequency	1 kHz
	Integrator	$g = 0.3$-0.6
	Rejection bandwidth	50–80 Hz
	Int. matrix	300 KL modes
NGS	Wavelength	850 nm
	Magnitude	7.5–13.5
	Photons/subap.	10–500
Telescope	Diameter	8 m
	Obstruction/Spider	None
	Resolution	160 px
DM	Actuator	357
	Geometry	Cartesian
	Inf. functions	Gaussian
	Coupling	35 per cent
PWFS	Sub-apertures	20 × 20
	Modulation	3 λ/D
	RON	None
	Photon noise	Yes
	Signal processing	Slopes-Maps
	Optical gains control	Yes[5]
SH WFS	Subapertures	20 × 20
	Pixel scale	0.22 arcsec
	RON	None
	Photon noise	Yes
	Signal processing	CoG

1996) and a Shack–Hartmann (SH) WFS (Hartmann 1900; Shack 1971) to investigate if the non-linearities of the PWFS can affect the tracking of the mis-registrations (Korkiakoski et al. 2008; Esposito et al. 2015; Deo et al. 2018; Fauvarque et al. 2019; Chambouleyron et al. 2020). This is because the sensitivity matrices required by the model (equation 9) are computed in a diffraction-limited regime that differs from the real operating point of the PWFS in which on-sky measurements are acquired.

In this analysis, we consider one push–pull measurement acquired every 0.05 s (every 50 frames, one push–pull measurement at 1 kHz is acquired), releasing the controller to apply the push–pull commands above the static DM correction.

4.1 Effect of the signal-to-noise ratio

In the first analysis, we study the effect of the S/N of the on-sky signals on the estimation of the parameters. We consider here an AO system with a SH WFS as the same results were obtained using a PWFS. As detailed in Section 3.2, the accuracy of the estimation depends on the amplitude, noise level and number of modes considered. We propose to consider a system with a static mis-registration of 20 per cent of a subaperture shift X and we investigate the accuracy reached by the algorithm for different noise regimes, amplitude of the signals and number of signals considered. We consider one, three and five PCA modes for each type of mis-registration, making the total number of modes acquired on-sky multiplied by a factor of 3 (rotation, shift X and shift Y).

Fig. 7 gives the estimation error of the algorithm for different S/N conditions. It shows that reducing the whole interaction matrix to a few well-selected modes allows us to extract the mis-registration parameters. The accuracy of the estimation depends both on the S/N of the signals (amplitude and number of measurement) and the

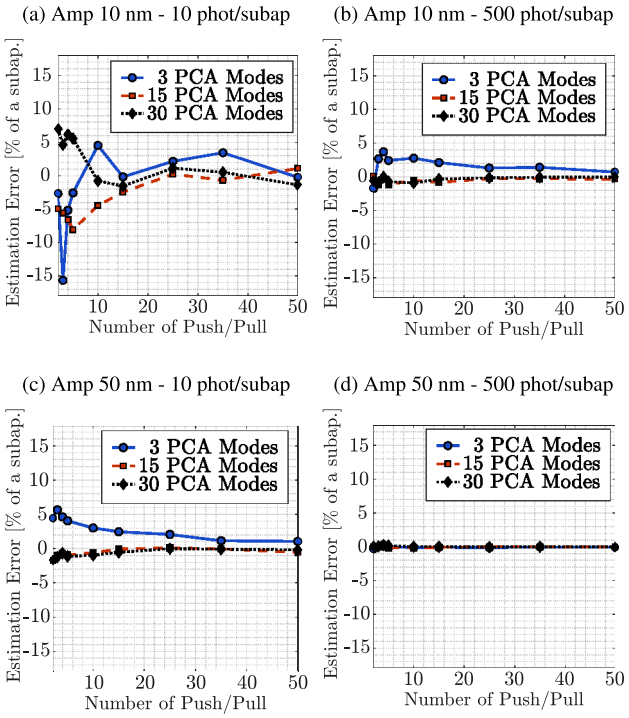

Figure 7. Accuracy of the algorithm on the estimation of a static shift X as a function of the number of push–pull measurements averaged. The results are shown for different S/N conditions (panels a–d) and for different number of modes acquired on-sky.

Table 2. Total number of averaged push–pull measurements required to reach convergence (<1 per cent of a subaperture) for the mis-registration estimation of a shift X in all the conditions of noise investigated (10 and 500 photons per subaperture per frame).

Amplitude a	30 modes	15 modes	3 modes
50 nm rms	300	150	100
10 nm RMS	>1500	>750	>150

number of modes considered. As expected, for a given S/N, the higher the number of modes, the better the accuracy.

This implies that by considering a larger number of modes, we can reduce the number of measurements required to reach convergence and we can obtain a better estimation of the parameters for a given S/N. However, the effect on the scientific path and the time required for the calibration becomes larger. Using the minimum number of modes (three PCA modes), Fig. 7 shows that with no more than 20 push–pull measurements, the method provides an accuracy better than 5 per cent of a subaperture in all the cases considered.

The results presented in the previous figures are summarized in Table 2, which gives the total number of push–pull measurements required to reach convergence for the estimation of a shift X of 20 per cent of a subaperture. To optimize the identification of the mis-registrations, a trade-off is required, using either many modes with a small number of measurements or using few modes with a larger number of measurements. Overall, the PCA modes allow us to reduce significantly the acquisition time necessary to measure the experimental signals required by the identification algorithm and to estimate accurately the mis-registration parameters. In the following, we always consider the use of three PCA modes and 50 push–pull

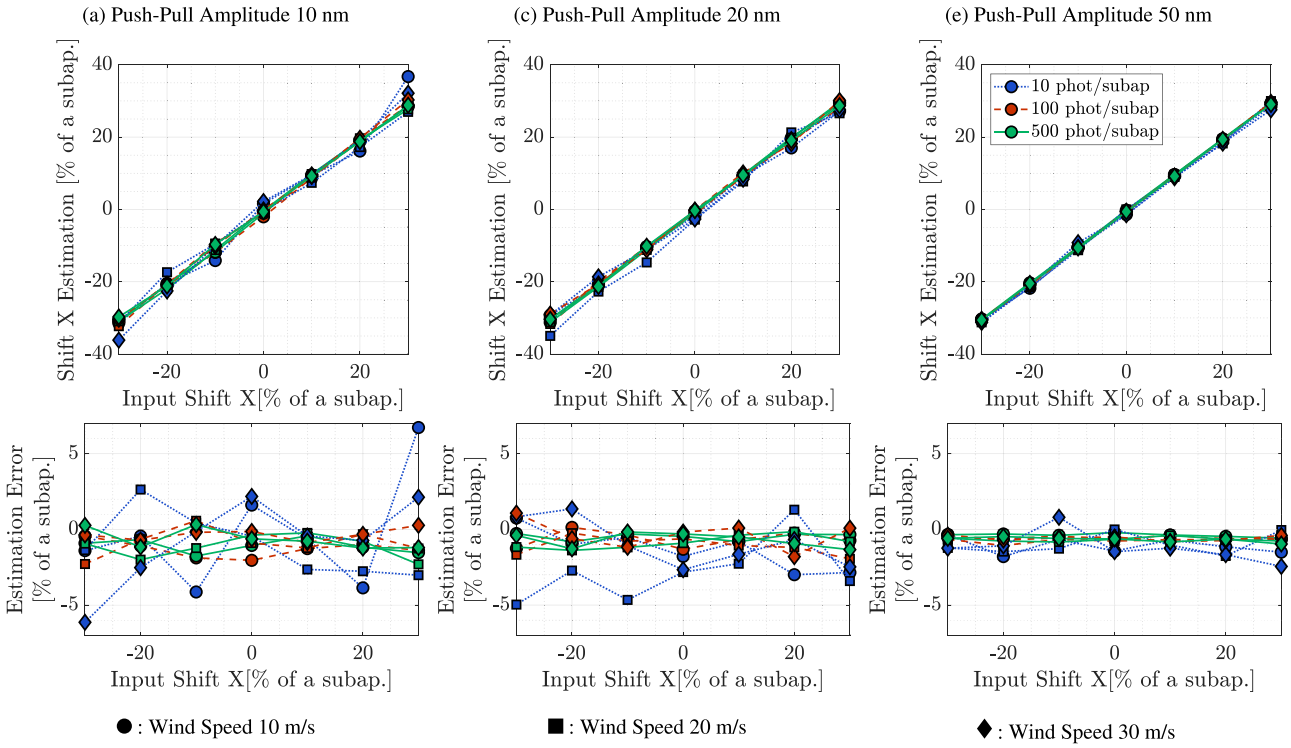

Figure 8. Shift X estimation using a PWFS (top) and corresponding estimation error (bottom) as a function of the input shift X for a push–pull amplitude of 10 nm (a), 20 nm (b) and 50 nm (c). The results are given for different noise regimes of 10, 100 and 500 photons per subaperture (dotted blue, dashed red and solid green lines, respectively). The markers correspond to different wind speeds of 10, 20 and 30 m s^{-1} (circles, squares and diamonds, respectively).

measurements to make sure that the estimation of the mis-registration parameters is close enough to the convergence value.

4.2 Ramps of mis-registrations

In the second analysis, we apply a ramp of a given mis-registration to a closed-loop AO system and acquire 50 push–pull measurements of three PCA modes (see Section 4.1). The mis-registrations applied here are chosen to maintain the system in a stable closed-loop regime (Fig. 1c).

To improve the readability of the paper, this section only shows the result corresponding to a PWFS. The same simulation results obtained with a SH WFS are provided in Appendix A and they show the same behaviour and performance. Figs 8 and 9 provide the mis-registration parameters estimation corresponding to a ramp of shift X and of rotation. For both cases and for all the closed-loop conditions explored (wind speed and noise regime), the accuracy reached with the method is very good, with a maximal error of 7 per cent of a subaperture for the shift and 0.6 degrees for the rotation. For both cases, this maximal error is obtained for the highest level of noise and smallest amplitude of push–pull. For this system, the shift on the border of the pupil corresponding to a rotation of 0.6 degrees is 10.5 per cent of a subaperture.

Excluding this specific case, the estimation reached by the method is well below the accuracy required: all the estimation errors are better than 5 per cent of a subaperture for the shift and better than 0.25 for the rotation. By considering the highest amplitude of push–pull and the lowest noise regime, we can improve the accuracy of the estimation to less than 1 per cent of a subaperture for the shift and less than 0.05 for the rotation.

These results are consistent with the considerations presented in the Section 3.2 and confirm the trends expected: the estimation of the parameters is more accurate when the S/N of the on-sky signal is higher. In particular, even for the lowest flux considered (10 photons per subaperture per frame), the method presented still provides a very accurate estimation of the parameter (under 5 per cent of a subaperture), adjusting the amplitude of the signals to 20 nm for example. In addition, the method appears to be robust to the different conditions of observation and to be independent of the mis-registration value to identify.

4.3 Multiple mis-registrations evolving dynamically

A more realistic situation is to apply multiple mis-registrations at the same time (rotation and shifts) evolving dynamically with time. In the following results, one iteration corresponds to one acquisition sequence of 50 push–pull measurements. We make the reasonable assumption that the mis-registrations remain static during one full acquisition sequence. The number of observing parameters considered is reduced to two different flux regimes for an amplitude of 20 nm rms and a wind speed of 15 m s^{-1} to limit the number of plots.

The results are provided for both a PWFS and SH WFS in Fig. 10, which shows that the estimation of mis-registration parameters in this realistic case is once again very accurate, with a maximum error of about 0.2 for the rotation and 2 per cent of a subaperture and most of the estimations better than 0.1 and 1 per cent shift error. This shows that the algorithm does not suffer from strong coupling between the parameters considered. In addition, the method performs equally for both WFSs.

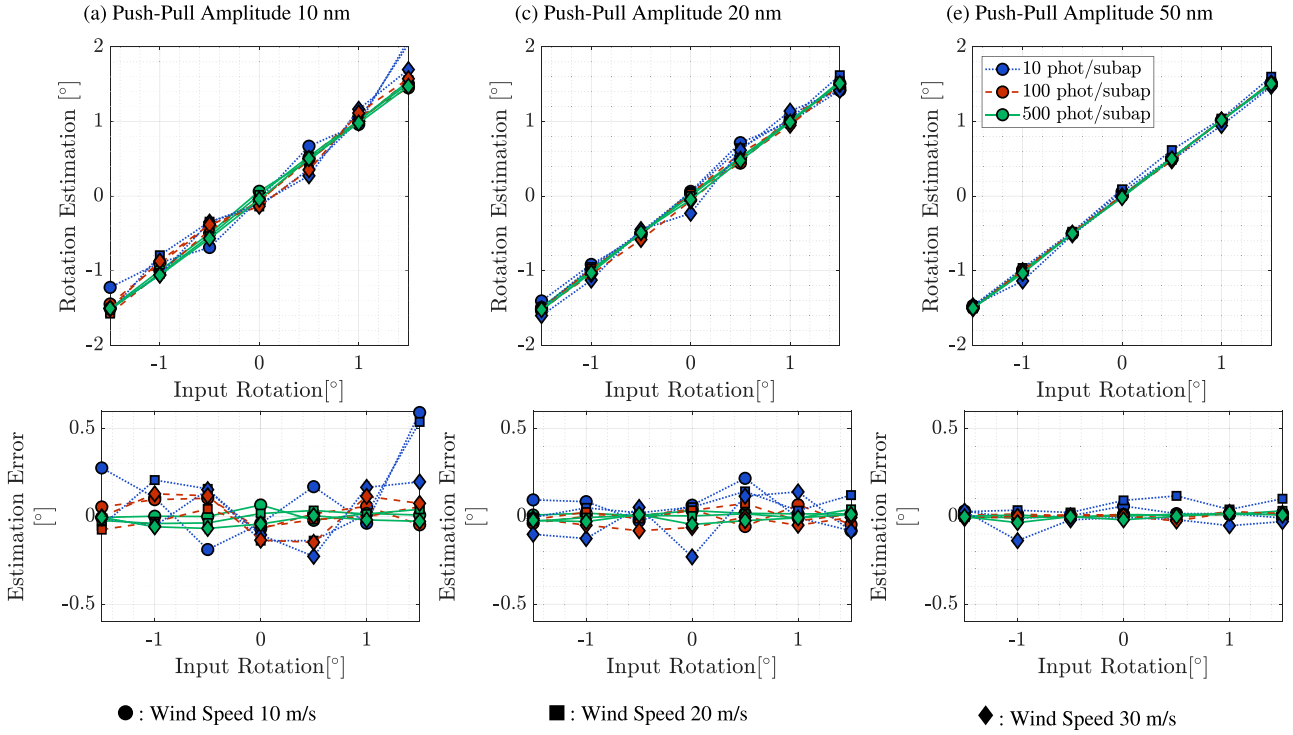

Figure 9. Rotation estimation using a PWFS (top) and corresponding estimation error (bottom) as a function of the input shift X for a push–pull amplitude of 10 nm (a), 20 nm (b) and 50 nm (c). The results are given for different noise regimes of 10, 100 and 500 photons per subaperture (dotted blue, dashed red and solid green lines, respectively). The markers correspond to different wind speeds of 10, 20 and 30 m s^{-1} (circles, squares and diamonds, respectively).

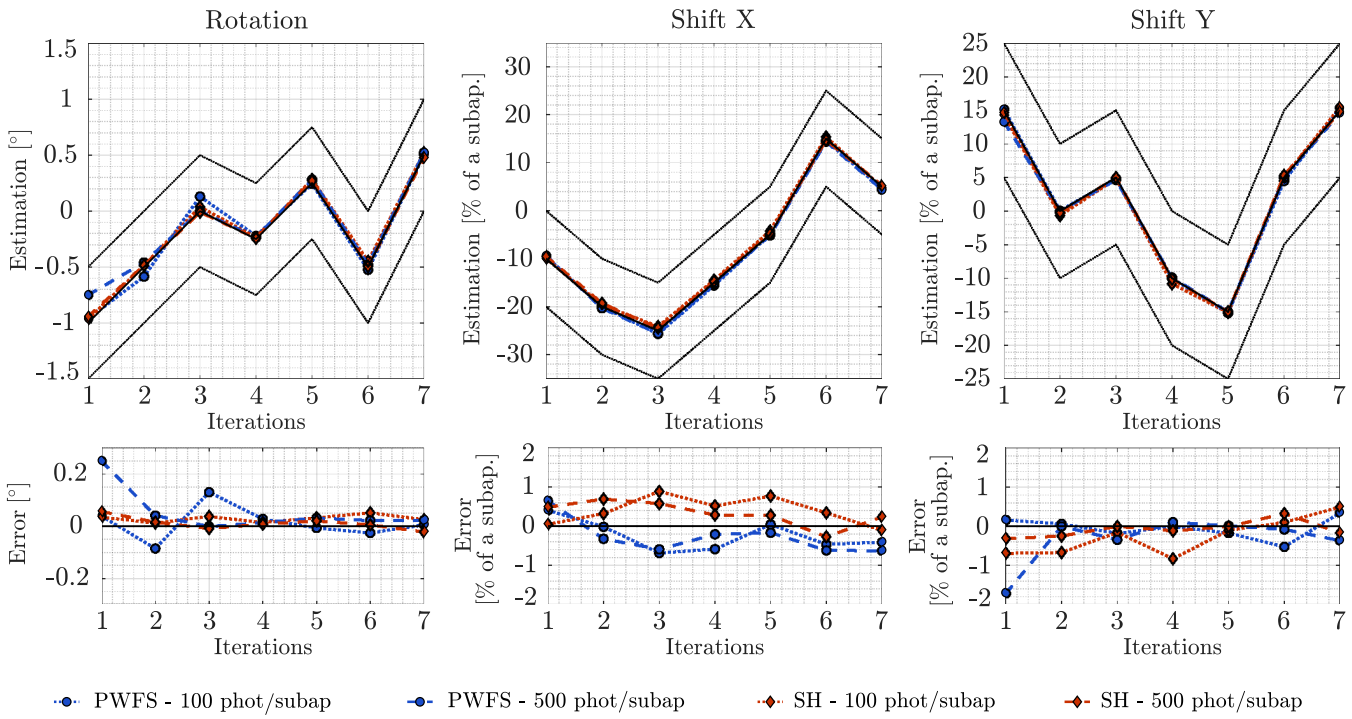

Figure 10. Estimation of mis-registration parameters (top) and corresponding estimation error (bottom) as a function of the number of iterations. The results are given for the rotation (left), shift X (middle) and shift Y (right). The black solid lines represent the actual true evolution of the mis-registration parameters and the dashed black lines are the accuracy target (10 per cent of a subaperture shift). The blue dashed lines represent the identified values of the mis-registration parameters when using a PWFS, while the red lines correspond to a SH WFS.

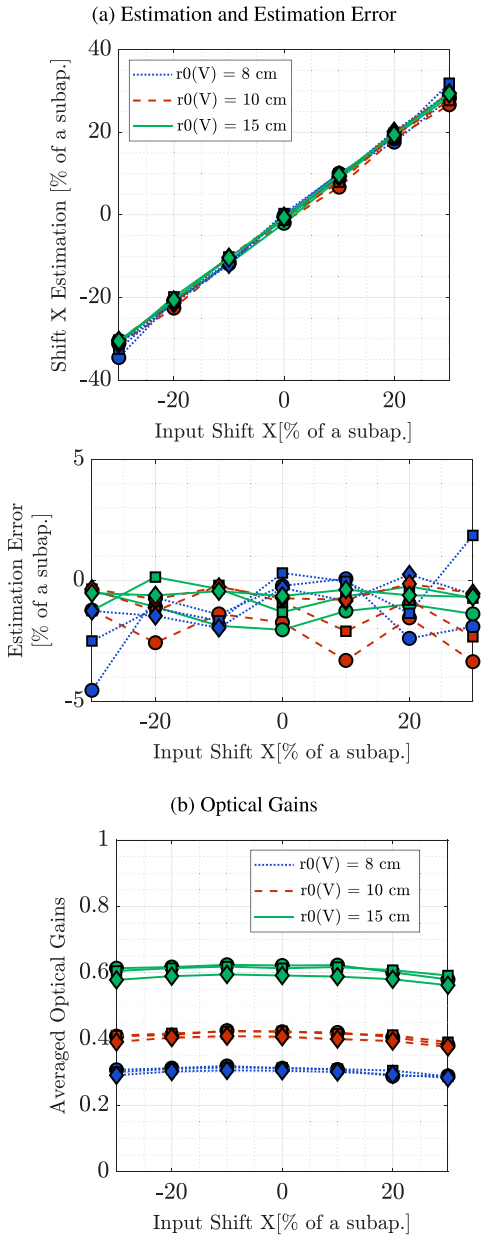

Figure 11. Shift X estimation and estimation error (a) and corresponding optical gains (b) as a function of the input shift X for different seeing conditions.The markers correspond to a push–pull amplitude of 10 nm (circles), 20 nm (squares) and 50 nm (diamonds).

4.4 Sensitivity to seeing conditions

In addition to the previous results, the algorithm has been validated against different seeing conditions to challenge the PWFS loss of sensitivity. This study does not include seeing variations during the acquisition of the signals. To limit the number of plots, we consider only a ramp of shift X for a wind speed of 10 m s^{-1} and a flux regime of 100 and 500 photons per subaperture. Once again, we consider 50 push–pull measurements.

In that case, the estimation of the mis-registration parameters and of the corresponding optical gains **G** for different values of the Fried parameter r_0 are provided in Fig. 11. In this figure, the markers correspond to different push–pull amplitudes (10, 20 and 50 nm rms). Fig. 11(a) shows that the algorithm is very robust against seeing variations, with a maximum error better than 5 per cent of a subaperture, which corresponds to the worst case considered (lowest r_0 value and lowest push–pull amplitude). As expected, the best estimation of the parameters is obtained for the largest r_0 value and largest push–pull amplitude. In that case, the maximum error is better than 1 per cent of a subaperture.

In addition, Fig. 11(b) gives the averaged optical gains identified by the algorithm (we consider here the averaged optical gains for the three PCA modes, e.g. the mean value of the diagonal of **G**). This plot shows that we retrieve the typical attenuation expected for mid-order modes of a modulated PWFS operating in the I band as a function of r_0 with an attenuation of 40 per cent, 60 per cent and 70 per cent for a Fried parameter of, respectively, 15, 10 and 8 cm in the visible (Deo et al. 2018). This plot also exhibits a slightly lower gain for larger values of mis-registrations. This is consistent with the fact that the AO residuals are slightly higher in the case of an imperfect DM/PWFS alignment, thus affecting the sensitivity of the PWFS.

Table 3. Summary of the cases considered to study the effect of the method in the scientific path. The units of the shifts applied (α_X and α_Y) are in percentage of a subaperture.

Case	Disturbance	Mis-registrations [α_{rot}, α_X, α_Y]	SR (H band)
0	None	[0°, 0%, 0%]	79.71
1	None	[0.3°, −15%, 20%]	78.25
2	None	[0.5°, −20%, 20%]	55.77
3	PCA_{rot}, 10 nm	[0°, 0%, 0%]	79.71
4	PCA_{rot}, 20 nm	[0°, 0%, 0%]	79.70
5	PCA_{rot}, 50 nm	[0°, 0%, 0%]	79.65
6	PCA_X, 10 nm	[0°, 0%, 0%]	79.71
7	PCA_X, 20 nm	[0°, 0%, 0%]	79.70
8	PCA_X, 50 nm	[0°, 0%, 0%]	79.65

4.5 Effect on the scientific path

4.5.1 Quantitative analysis

The purpose of this section is to quantify the cost of applying the push–pull measurements on the scientific path taking the cases presented in Sections 4.2, 4.3 and 4.4 using 50 push–pull measurements every 50 frames at 1 kHz of one given PCA mode. The summary of the cases considered with the corresponding long-exposure Strehl ratio (SR) is given in Table 3. We limit the study to one PCA mode at a time corresponding to the rotation (cases 3–5 in Table 3) and to the shift X (cases 6–8 in Table 3) with different push–pull amplitudes. Based on the results presented in the previous section, we assume that the mis-registration monitoring strategy allows us to perfectly compensate for the mis-registrations so that the system with disturbance is operating around its nominal working point and only suffers from the perturbation introduced by the PCA modes. The reference case for the nominal performance consists of a closed-loop system with no disturbance applied and no mis-registration (case 0 in Table 3). In addition, we propose to compare the effect of our invasive strategy with respect to a small and a large mis-registration (cases 1 and 2 in Table 3) that remains uncorrected.

Table 3 shows that the disturbances have a negligible effect on the performance of the AO system with a maximum loss of 0.05 per cent of Strehl ratio in the H band in the worst case (larger amplitude of the signals). As a comparison, the mis-registrations considered cause a loss of 0.75 per cent and 15 per cent of Strehl ratio.

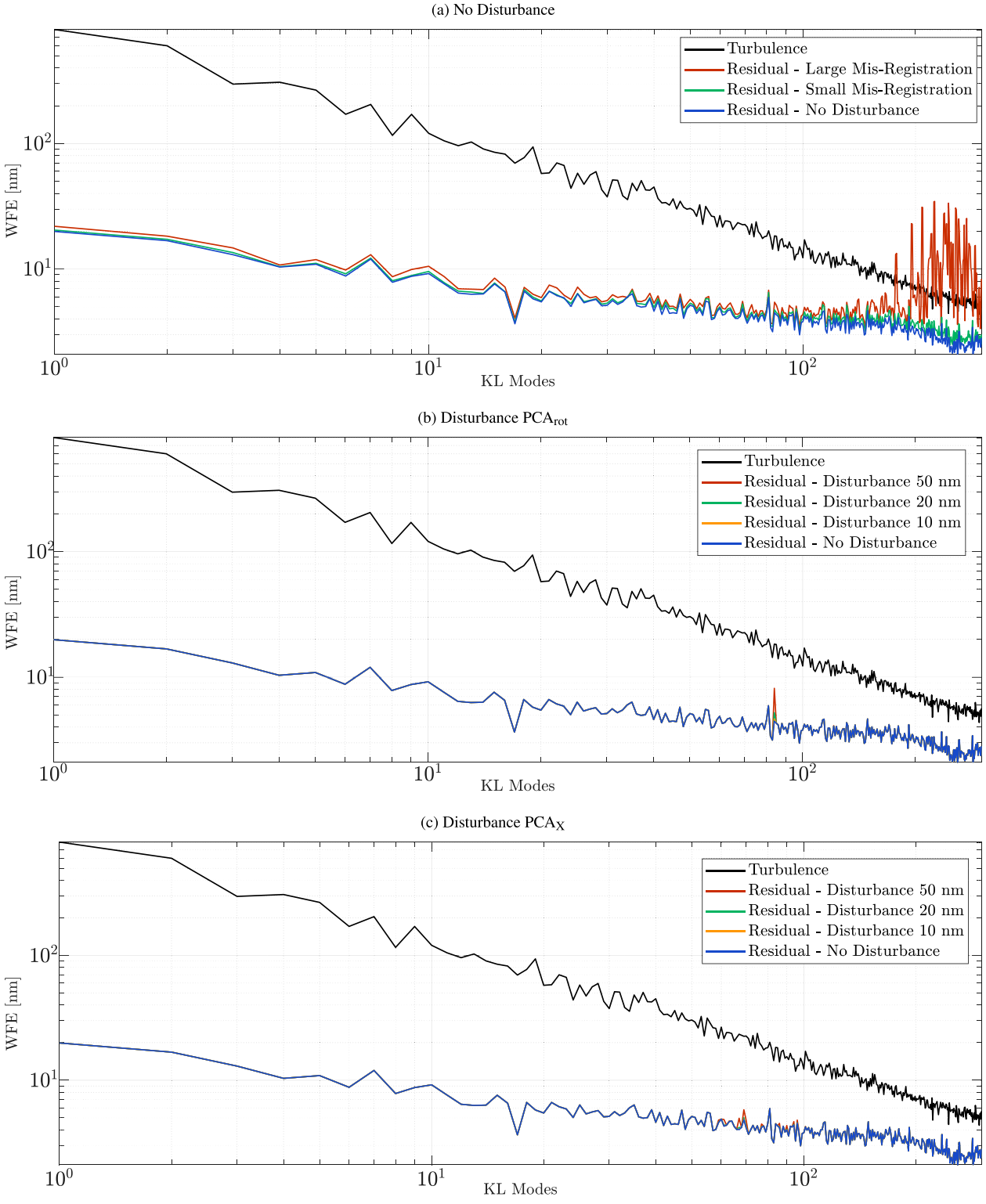

Figure 12. Modal PSD corresponding to the cases of Table 3. The open-loop turbulence (solid black line) and reference case (solid blue line) are given for each plot.

To provide a more detailed analysis, the modal PSD corresponding to the different cases considered in Table 3 are provided in Fig. 12. This figure confirms the performance presented in Table 3, exhibiting a strong effect of the mis-registrations and a negligible effect of the disturbance applied using PCA modes. In particular, we clearly identify that the disturbance due to the actuation of the PCA modes is very localized on one or a few modes. For low push–pull amplitudes, the effect is even hardly visible on the modal PSD as the curves overlap (Figs 12a and 12b). On the contrary, the effect of uncompensated mis-registrations affects all

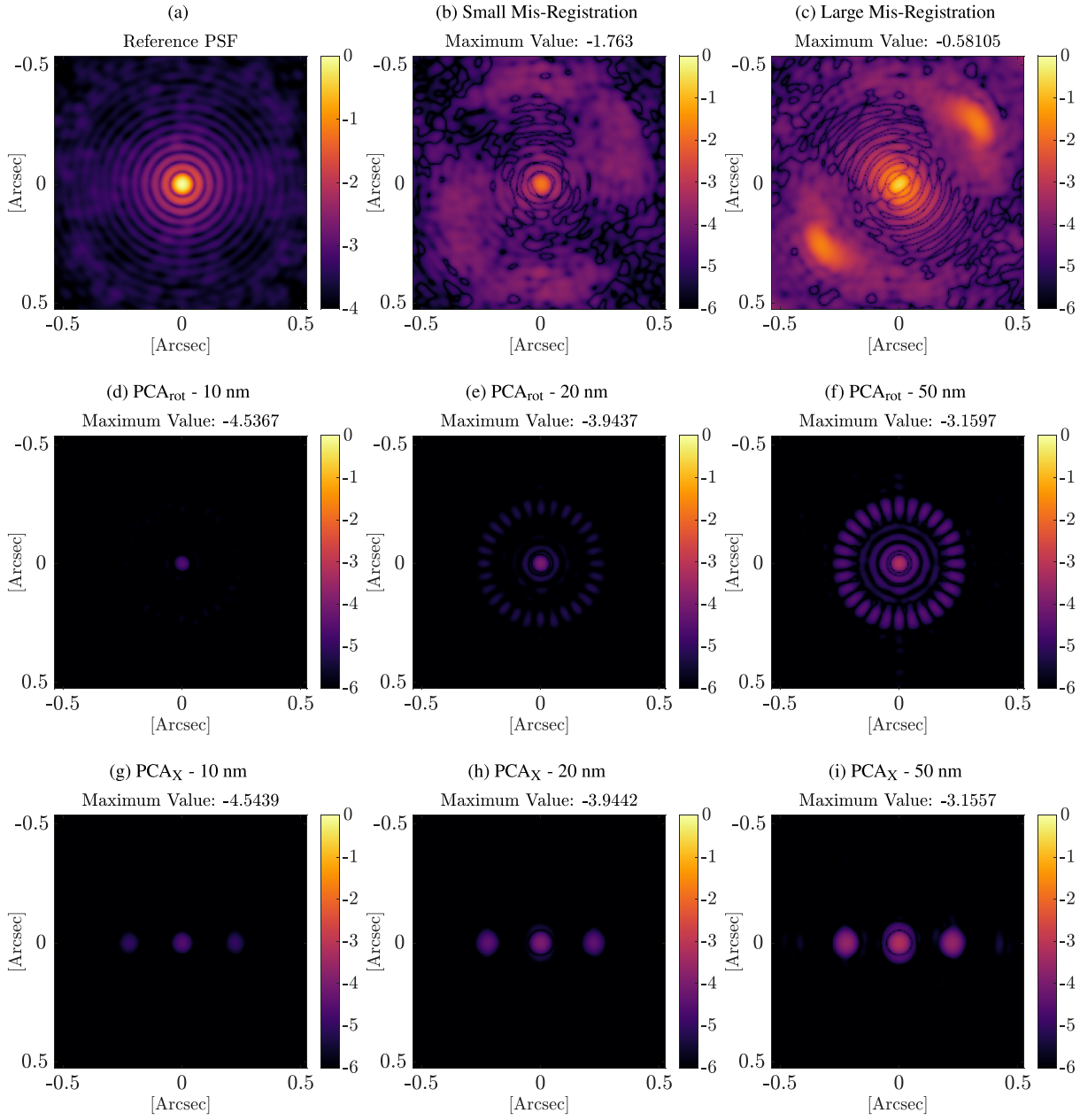

Figure 13. Comparison of the effect on the PSF. (a) Normalized *H*-band PSF (in logarithm scale) corresponding to the reference case. (b)–(i) Difference between the reference PSF and the cases listed in Table 3.

the modes and is clearly visible on the modal PSD (Fig. 12a). In the case of large mis-registrations, we retrieve the behaviour introduced in Fig. 12(a) with instabilities for the higher spatial frequencies.

In addition, the corresponding effects on the scientific PSF are provided in Fig. 13. We consider a long-exposure closed-loop PSF in the *H* band (2.5-s integration at 1 kHZ with no source of noise) as a reference. This reference PSF is normalized to 1 and all the other PSFs are normalized using the same normalization factor to provide a relative comparison with respect to this nominal case. The PSF displayed in Figs 13(b)–(f) correspond to the difference between the reference PSF (Fig. 13a) and the PSF obtained in the different cases listed in Table 3. For each case, the maximum value of the residual PSF is indicated.

This figure shows that the effects of the mis-registrations considered are to be very visible inside the correction zone of the PSF. The shape of the PSF results appear to be altered, especially in the case of a large mis-registration where the maximum value of the delta PSF is around $10^{-0.6}$. In contrast, the effect of the disturbance applied using the PCA modes appears to be of a much smaller amplitude with a maximum value of about 10^{-3} for the highest amplitude. This represents a factor of 1000 with respect to the small mis-registered case and this factor goes to 10 000 when considering the smallest push–pull amplitude. Fig. 3 allows us also to quantify clearly how the PSF is spatially affected by the modes selected as a function of the amplitude of the signal.

The results provided in this section make us confident about using the proposed measurement strategy even during the observation, as

the effect on the observation appears negligible. This conclusion is, however, system-dependent and the effect should be carefully evaluated beforehand. In the next section, we define a methodology to select the modes used to track the mis-registrations.

4.5.2 Qualitative analysis

Section 4.5.1 has shown that the effect of the perturbation introduced in the scientific path depends on the amplitude and spatial properties of the signals. In terms of operation, the choice of the signal properties has to be tailored to the observing conditions (perhaps, e.g., the level of noise, turbulence or the level of AO correction), on the accuracy requirements and on the type of scientific observation (perhaps, e.g., the effect on the focal plane or on the performance). The measurement strategy results then in a trade-off between all these different considerations and it will be system-dependent. Here, we define a methodology to identify the modes that are the most relevant to estimate the mis-registrations. We recall the expression of the measurement noise $\boldsymbol{\xi}_k$:

$$\boldsymbol{\xi}_k = \frac{-\mathbf{M}_{\mathrm{WFS}} \cdot \boldsymbol{\delta\phi}_k^{\mathrm{res}} + \boldsymbol{\eta}_k - \boldsymbol{\eta}_{k+1}}{2a}. \tag{28}$$

The procedure should include:

(i) the definition of the requirements in terms of accuracy for the mis-registration parameters with a sensitivity analysis of the system (see Fig. 1);

(ii) the identification of the observing conditions, such as the level of noise $\boldsymbol{\eta}$, level of turbulence $\boldsymbol{\delta\phi}^{\mathrm{res}}$ and level of AO correction;

(iii) the investigation of the effect on the science path (e.g. the effect of the modes on the PSF, AO performance, and acquisition time T allocated to identify the parameters) to identify the constraints for the amplitude a and the spatial properties of the modes considered;

(iv) the determination of the trade-off between number of modes N_{modes}, the acquisition time allocated T, and amplitude a required to reach the accuracy targeted.

If the amplitudes of the modes are small (typically 20 nm rms), and talso he measurement time required (hundreds of frames for a few PCA modes), the effect will be negligible on long-exposure PSFs, as shown in Section 4.5.1. By contrast, if higher amplitudes are required, the dithering could be applied during the read-out time of the detectors, when the scientific shutter is closed. This would provide a way to regularly acquire high S/N signals during the operations without affecting the scientific path.

5 CONCLUSION

To address the question of a regular tracking of the DM/WFS mis-registrations during scientific operations, we have introduced a strategy based on an invasive approach. This strategy is inspired from the state of the art in terms of on-sky calibration and consists of applying these calibration techniques (modulation/demodulation) to a few well-selected modes and estimating from them the mis-registration parameters. We have demonstrated that the method is applicable for both the SH WHS and PWFS, as the algorithm includes a compensation for the PWFS optical gains.

Our research is oriented to minimize the number of modes required by the algorithm in order to estimate accurately the mis-registration parameters. This is by identifying the most sensitive modes to the mis-registrations using a PCA of the sensitivity interaction matrices.

Using on-sky push–pull measurements, we investigated the accuracy achieved with only three PCA modes, exploring different observing conditions. Even in very low flux conditions, it is always possible to tune the push–pull amplitude and the measurement time to reach a very good estimation accuracy. In addition, it has been shown that the effect of these on-sky disturbances on the quality of the science PSF is fully negligible.

Finally, we have demonstrated that this procedure is performing extremely well for various mis-registrations evolving dynamically at the same time. By using only three PCA modes with an amplitude of 20 nm rms, we can provide a tracking of the mis-registration parameters with an accuracy better than 1 per cent of a subaperture.

A future step in this work will require an experimental validation of the method, implementing it on an existing facility equipped with a secondary adaptive mirror. In addition, it will be relevant to investigate if this calibration strategy allows us to retrieve other parameters such as optical gains for the PWFS, for instance to compensate properly non-common path aberrations (Esposito et al. 2020).

In addition, it will be necessary to study how this novel method performs, taking into account more complex closed-loop effects specific to large adaptive telescopes equipped with a large adaptive secondary mirror. The couplings with pupil fragmentation effects, due to the presence of thick spiders, deformable mirror saturation and the segmentation of the primary mirror, will have to be investigated. In particular, in this paper, we put light on the coupling between the optical gains of the PWFS and the presence of mis-registrations. In the context of the ELT, PWFS optical gains are expected to exhibit large variations (Deo et al. 2018), which will require aggressive compensation strategies (Deo et al. 2019a, 2021). An accurate tracking and compensation of the mis-registration will be required to prevent any bias in the optical gains estimation that would lead to loop instabilities or over/under compensation of non-common path aberrations (Esposito et al. 2020).

ACKNOWLEDGEMENTS

We thank the referee for constructive comments that helped to improve the paper. This document has been prepared as part of the activities of OPTICON H2020 (2017–2020) Work Package 1 (Calibration and test tools for AO assisted E-ELT instruments). OPTICON is supported by the Horizon 2020 Framework Programme of the European Commission (grant number 730890). This work was also supported by the Action Spécifique Haute Résolution Angulaire (ASHRA) of CNRS/INSU co-funded by CNES, and benefited from the support of the WOLF project ANR-18-CE31-0018 of the French National Research Agency (ANR).

DATA AVAILABILITY

The data and simulation code underlying this article will be shared on reasonable request to the corresponding author.

REFERENCES

Arsenault R. et al., 2008, Proc. SPIE, 7015, 701524
Béchet C., Tallon M., Thiébaut E., Kolb J., Madec P.-Y., 2011, in Second International Conference on Adaptive Optics for Extremely Large Telescopes (AO4ELT II), paper 61, available online at http://ao4elt2.lesia.obspm.fr
Béchet C., Tallon M., Thiébaut E., 2012, Proc. SPIE, 8447, 84472C
Bertrou-Cantou A. et al., 2020, Proc. SPIE, 11448, 1144812
Biasi R., Gallieni D., Salinari P., Riccardi A., Mantegazza P., 2010, Proc. SPIE, 7736, 77362B
Bonnefond S., Tallon M., Le Louarn M., Madec P.-Y., 2016, Proc. SPIE, 9909, 990972

Bonnet H. et al., 2018, Proc. SPIE, 10703, 1070310
Boyer C., Michau V., Rousset G., 1990, Proc. SPIE, 1271, 63
Briguglio R. et al., 2018a, Scientific Reports, 8, 1
Briguglio R., Pariani G., Xompero M., Riccardi A., Tintori M., Gallieni D., Biasi R., 2018b, Proc. SPIE, 10703, 1070379
Chambouleyron V., Fauvarque O., Janin-Potiron P., Correia C., Sauvage J.-F., Schwartz N., Neichel B., Fusco T., 2020, A&A, 644, A6
Cheffot A.-L., Vigan A., Lévêque S., Hugot E., 2020, Optics Express, 28, 12566
Chiuso A., Muradore R., Marchetti E., 2010, IEEE Trans. Control Systems Technology, 18, 705
Cirasuolo M. et al., 2018, The Messenger, 171, 20
Conan R., Correia C., 2014, Proc. SPIE, 9148, 91486C
Deo V., Gendron É., Rousset G., Vidal F., Buey T., 2018, Proc. SPIE, 10703, 1070320
Deo V. et al., 2019a, in Proc. AO4ELT6 on Adaptive Optics for Extremely Large Telescopes, Available at: http://ao4elt6.copl.ulaval.ca/proceedings/401-2dxt-251.pdf
Deo V., Gendron É., Rousset G., Vidal F., Sevin A., Ferreira F., Gratadour D., Buey T., 2019b, A&A, 629, A107
Deo V. et al., 2021, preprint (arXiv:2103.09921)
Esposito S., Pinna E., Puglisi A., Agapito G., Veran J., Herriot G., 2015, in Proc. AO4ELT4 on Adaptive Optics for Extremely Large Telescopes, Available at: https://doi.org/10.20353/K3T4CP1131573
Esposito S., Puglisi A., Pinna E., Agapito G., Quirós-Pacheco F., Véran J., Herriot G., 2020, A&A, 636, A88
Fauvarque O., Janin-Potiron P., Correia C., Brûlé Y., Neichel B., Chambouleyron V., Sauvage J.-F., Fusco T., 2019, J. Opt. Soc. Am. A, 36, 1241
Fusco T., Conan J., Rousset G., Mugnier L., Michau V., 2001, J. Opt. Soc. Am. A, 18, 2527
Gendron E., 1995, PhD thesis, Université Denis Diderot – Paris VII
Gilmozzi R., Spyromilio J., 2007, The Messenger, 127, 11
Hartmann J., 1900, Zeitschrift für Instrumentenkunde, 20, 47
Heritier C. T. et al., 2018a, Proc. SPIE, 10703, 107034P
Heritier C. T. et al., 2018b, MNRAS, 481, 2829
Kolb J., Madec P.-Y., Louarn M. L., Muller N., Béchet C., 2012, Proc. SPIE, 8447, 84472D
Korkiakoski V., Vérinaud C., Le Louarn M., 2008, Appl. Opt., 47, 79
Lai O., Chun M., Dungee R., Lu J., Carbillet M., 2021, MNRAS, 501, 3443
Le Louarn M., Madec P.-Y., Marchetti E., Bonnet H., Esselborn M., 2016, Proc. SPIE, 9909, 990975
Madec P.-Y., 2012, Proc. SPIE, 8447, 844705
Marquardt D. W., 1963, J. Soc. Industrial and Applied Mathematics, 11, 431
Meimon S., Delavaquerie E., Cassaing F., Fusco T., Mugnier L. M., Michau V., 2008, Proc. SPIE, 7012, 701214
Neichel B., Parisot A., Petit C., Fusco T., Rigaut F., 2012, Proc. SPIE, 8447, 84475N
Oberti S., H Bonnet H., Fedrigo E., Ivanescu L., Kasper M., Paufique J., 2004, Proc. SPIE, 5490, 139
Oberti S. et al., 2006, Proc. SPIE, 6272, 627220
Oberti S. et al., 2018, Proc. SPIE, 10703, 107031G
Pearson K., 1901, The London, Edinburgh, and Dublin Philosophical Magazine and Journal of Science, 6, 559
Pieralli F., Puglisi A., Quirós-Pacheco F., Esposito S., 2008, Proc. SPIE, 7015, 70153A
Pinna E. et al., 2012, Proc. SPIE, 8447, 84472B
Ragazzoni R., 1996, J. Mod. Opt., 43, 289
Riccardi A. et al., 2010, Proc. SPIE, 7736, 77362C
Schwartz N. et al., 2018, Proc. SPIE, 10703, 1070322
Shack R. V., 1971, J. Opt. Soc. Am., 61, 656
Southwell W. H., 1980, J. Opt. Soc. Am., 70, 998
Vernet E., Cayrel M., Hubin N., Mueller M., Biasi R., Gallieni D., Tintori M., 2012, Proc. SPIE, 8447, 844761
Vernet E., Cayrel M., Hubin N., Biasi R., Gallieni D., Tintori M., 2014, Proc. SPIE, 9148, 914824
Wallner E., 1983, J. Opt. Soc. Am., 73, 1771

APPENDIX A: COMPLEMENTARY RESULTS WITH A SH WFS

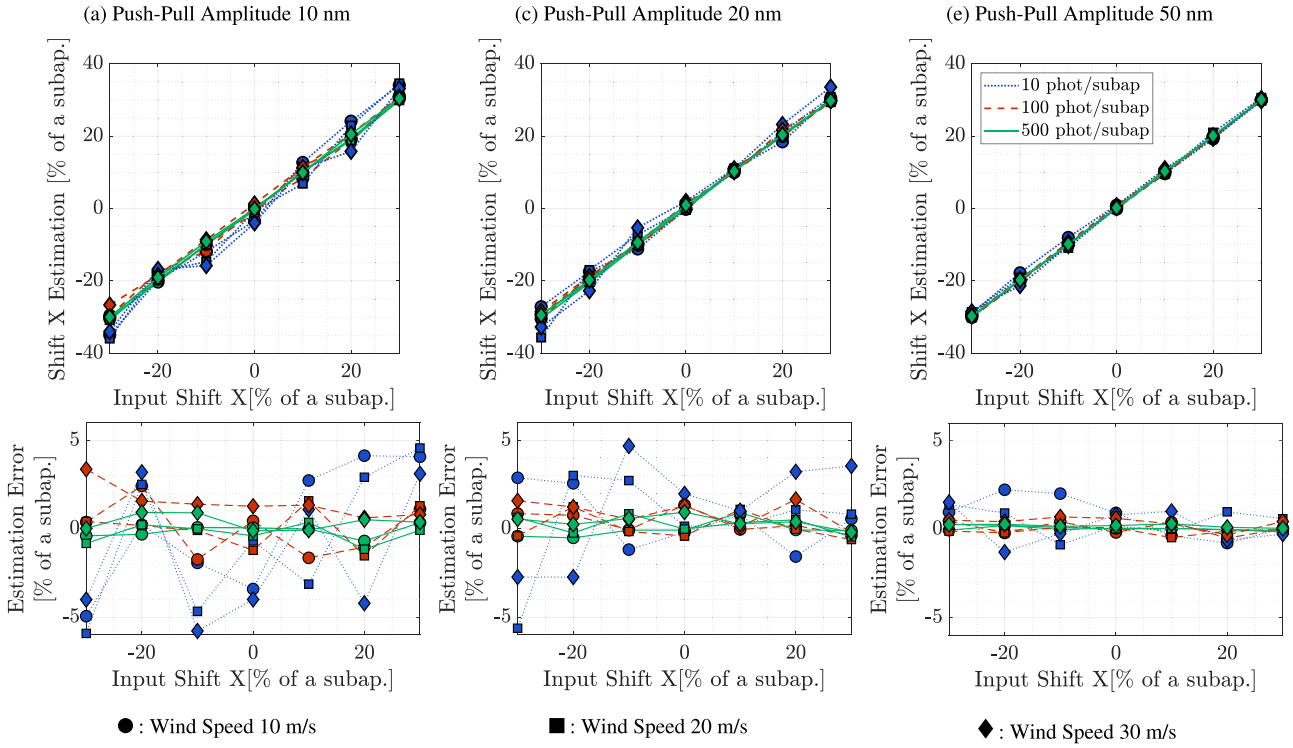

Figure A1. Shift X estimation (top) and corresponding estimation error (bottom) as a function of the input shift X for a push-pull amplitude of 10 nm (a), 20 nm (b) and 50 nm (c) using a SH-WFS. The results are given for different noise regimes of 10, 100 and 500 photons per subaperture (dotted blue, dashed red and solid green lines, respectively). The markers correspond to different wind speeds of 10, 20 and 30 m s^{-1} (circles, squares and diamonds, respectively).

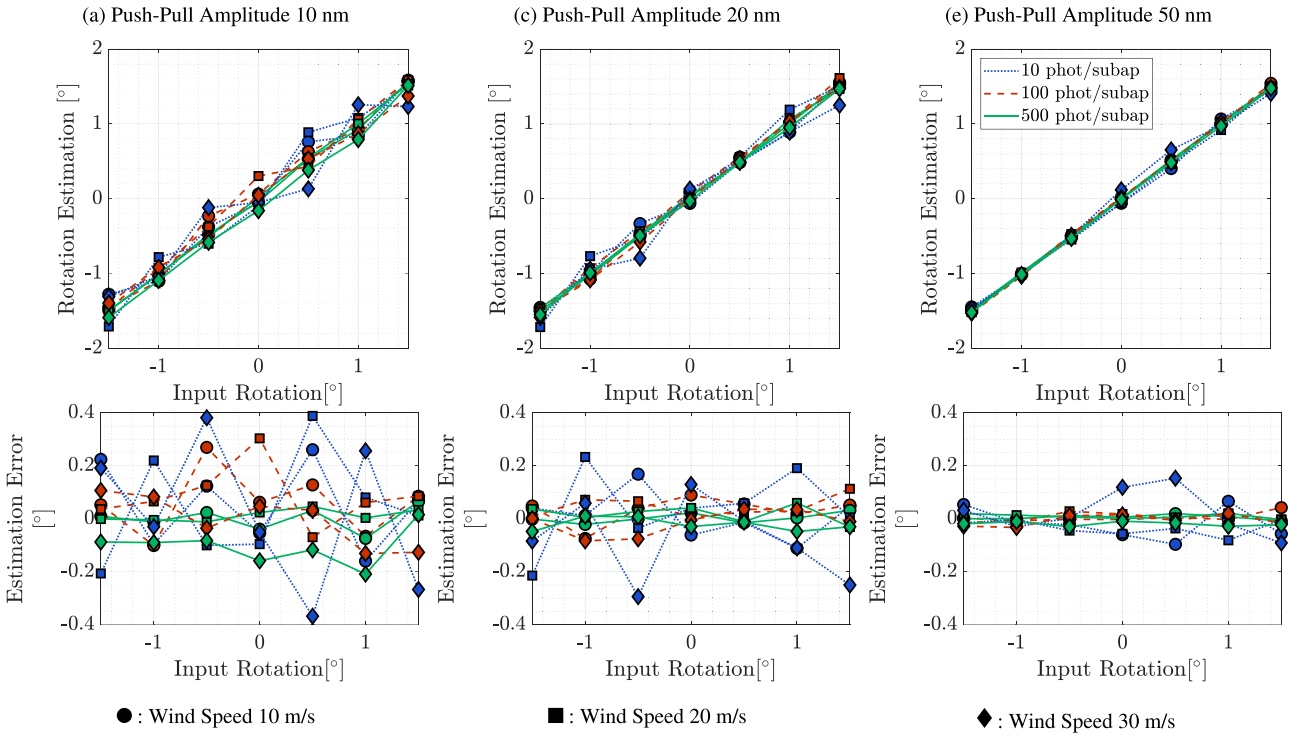

Figure A2. Rotation estimation (top) and corresponding estimation error (bottom) as a function of the input shift X for a push–pull amplitude of 10 nm (a), 20 nm (b) and 50 nm (c) using a SH WFS. The results are given for different noise regimes of 10, 100 and 500 photons per subaperture (dotted blue, dashed red and solid green lines, respectively). The markers correspond to different wind speeds of 10, 20 and 30 m s^{-1} (circles, squares and diamonds, respectively).

This paper has been typeset from a TEX/LATEX file prepared by the author.